An investigation into the role that a transverse magnetic field plays in the formation of large anode sheath potentials

J. E. Foster[a] and A. D. Gallimore[b]
The Plasmadynamics and Electric Propulsion Laboratory, The University of Michigan, Ann Arbor, Michigan 48109

(Received 6 February 1996; accepted 23 July 1996)

A 9.25 A low-pressure (45–55 mTorr) hollow cathode arc discharge has been used to simulate plasma processes that occur at the anode of magnetoplasmadynamic accelerators used for space propulsion applications. The interest in the near-anode region is related to findings of past research, which indicate that large anode sheath potentials can drive as much as 70% of the input electrical power into the anode, thus degrading thrust efficiency. Presented here are results that essentially characterize the behavior of the near-anode plasma as a function of a transverse magnetic field. Plasma diagnostics included single Langmuir probe techniques, emission spectroscopy, and water calorimetry for anode heat flux measurements. Phenomenological arguments based on measurements taken suggest that observed changes in anode fall voltage are related to variations in the measured local electron number density as the magnetic field is varied. This behavior is attributed to the variations in the measured ionization rate, which is shown to be a nonlinear function of transverse magnetic field. © *1996 American Institute of Physics.* [S1070-664X(96)00311-4]

I. INTRODUCTION

The purpose of this study is to characterize the effect that a transverse magnetic field has on near-anode plasma properties. The basis of the research is essentially connected to fundamental problems facing designers of various plasma accelerators. More specifically, the plasma accelerators referred to here are used primarily for space propulsion applications such as satellite station keeping, orbit transfer, and primary propulsion. This field, known as electric propulsion, is essentially a facet of rocket science that deals with engines that generate thrust through electrical means. These systems are generally categorized into three areas depending on how the thrust is generated: (1) electrothermal, (2) electrostatic, and (3) electromagnetic. Because a number of these systems utilize nonzero $\mathbf{E}\times\mathbf{B}$ geometries to generate thrust, the need to understand specific plasma–electrode interactions under transverse magnetic field conditions naturally arises. Understanding processes that go on at the electrodes is particularly important, in that it yields information on engine lifetime, which is related to erosion phenomena occurring at the electrodes, and on engine efficiency, which is related to energy loss phenomena occurring at the electrodes.

The present research is geared toward understanding the role that the transverse magnetic field plays in driving energy loss processes at the anode. Past studies done on the electromagnetic thruster known as the magnetoplasmadynamic (MPD) thruster have shown that power losses to the anode can be as high as 70% of the input discharge power.[1] Power losses at the anode of MPD thrusters has been shown to be related to the magnitude of the transverse magnetic field component inside the discharge chamber.[2] Schall investigated the effect of magnetic field orientation relative to the anode on anode fall voltage and on anode power deposition in a MPD thrusters.[3] In addition, Tahara *et al.* studied the effect of an axial magnetic field on thrust production and thruster discharge stability.[4] Gallimore *et al.* correlated anode fall growth with increases in the near-anode Hall parameter, a ratio of the electron cyclotron frequency to the electron collison frequency, in a self-field pulsed MPD thruster.[2] More recently, Scheuer *et al.* utilized an applied-field magnetic nozzle to significantly reduce anode fall voltage in a MPD device.[5] The present work seeks to investigate the effect that a transverse magnetic field has on sheath potentials at the current collecting anode using a low-pressure diode configuration to simulate near-anode conditions similar to the 100 kW class MPD engine. The relevance of this study to MPD research is related to the fact that the self-field or the applied axial magnetic field present in MPDs are both perpendicular to current flow, as is simulated in this investigation. An understanding of the behavior of the near-anode plasma under these conditions is important in that it can provide insight into why the large anode sheath voltages develop in the first place.

This study is primarily a continuation of the near-anode, ''free burning'' arc studies conducted at the National Aeronautics and Space Administration's Lewis Research Center by Soulas and Myers.[6] Their work was essentially a preliminary examination of plasma–anode interactions with the main focus resting upon identifying the effects of magnetic field (both direction and magnitude) and local gas pressure on measured anode power flux and on estimated anode fall voltage. The research in this present work, however, concentrates on how plasma properties themselves are related to the formation and growth of the anode fall voltage as a function of transverse magnetic field with the objective being to relate this microscopic viewpoint to the macroscopic one, which includes an understanding of anode power deposition in actual MPD thrusters. Presented here are findings based on phenomenological arguments that relate changes in near-anode electron number density with the evolution of anode

[a]Graduate Assistant in Applied Physics.
[b]Assistant Professor of Aerospace Engineering and Applied Physics.

sheath voltage. In addition to electrostatic probe and emission spectroscopy measurements, also presented are calorimetric measurements of the magnitude of anode power deposition as a function of transverse magnetic field. Changes in measured anode power deposition are also correlated to changes in the anode sheath voltage.

Our experimental approach to studying the problem of the anode sheath in a magnetic field is unique in comparison to previous studies in that it allows the problem to be studied from a vantage point that is independent of other phenomena that would otherwise convolute the findings with influences from other effects (i.e., plasma acceleration). Essentially all previous studies have been done using pulsed MPD engines. In this investigation, near-anode processes are investigated under steady-state conditions; as a result, transient phenomena that are associated with pulsed discharges do not complicate interpretation. In addition, the findings of this study are independent of engine geometry. Previous studies concentrate on anode fall behavior as a function of thruster parameters. In this respect, the picture is macroscopic with little emphasis placed on characterizing the changes in the near-anode plasma properties. For the most part, many of these studies attribute the depletion of charge carriers as the main reason for anode fall growth.[3,7] In this study, the changes in the charge carriers in the near-anode region are characterized as a function of the transverse magnetic field. In this respect, this study investigates long held suspicions concerning near-anode charge carrier depletion and the associated growth in the anode fall region as a function of the transverse magnetic field using an apparatus that is well adapted for parametric studies. Another important aspect of this study is related to the fact that the experimental setup allows for the study of the variations of the near-anode plasma as a function of the transverse magnetic field at a fixed discharge current. In pulsed, self-field thruster studies, the magnitude of the magnetic field cannot be varied independently of the discharge current.

II. THEORY AND MOTIVATION

As mentioned earlier, an understanding of why the large anode sheath potentials arise and grow with transverse magnetic field is important to the electric propulsion community. Such large potentials give rise to lower engine performance because power that could be channeled into thrust production processes is instead deposited into the anode as waste heat.

In general, the potential distribution that defines the magnitude and sign of the anode fall region is determined by the space charge distribution in the near-anode region through Poisson's equation. The transverse electron flux at the anode sheath boundary in turn determines the steady-state space charge distribution throughout the anode sheath. This transverse flux, Γ_e, is ultimately controlled by the transverse magnetic field:

$$\Gamma_e = -D_\perp \cdot \frac{dn_e}{dz}, \tag{1}$$

where the transverse diffusion coefficient, $D_\perp$, is represented classically by

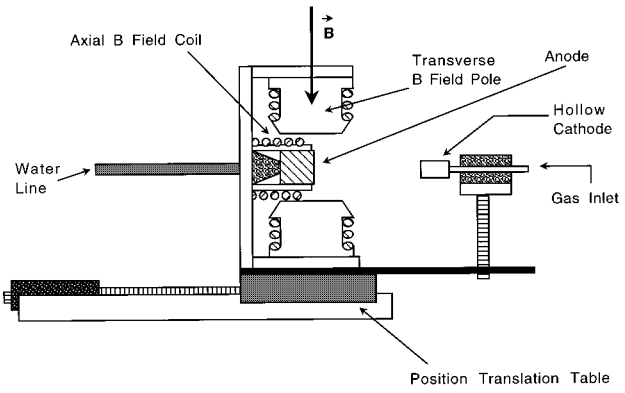

FIG. 1. Experimental apparatus.

$$D_\perp = \frac{D}{1+\omega_{ce}^2/\nu^2}, \tag{2}$$

though for many experiments the empirically derived relation of Bohm better describes the experimental observations:

$$D_\perp = \frac{kT_e}{16 \cdot eB}, \tag{3}$$

where dn_e/dz is the electron density gradient, ω_{ce} is the electron cyclotron frequency, ν is the electron collision frequency, k is Boltzmann's constant, T_e is the electron temperature, e is the elementary charge, D is the diffusion coefficient, and B is the transverse magnetic field. It is this relationship between the magnetic field and transverse flux that ultimately controls the anode fall voltage.

The plasma discharge can be expected to be stable as long as the ratio of the available current from the plasma, $e \cdot \Gamma_e \cdot A$, where A is the effective electrode collection area, to the discharge current, I_d, is of order unity or greater. In order to test the above mentioned assertions, Langmuir probes have been employed to measure electron number density and the corresponding anode fall voltage as a function of transverse magnetic field. The probes are also used to make electron energy distribution measurements so that ionization rates can be calculated. Correlations in the calculated ionization rates and transverse magnetic field can be in turn related to changes in anode fall voltages. Emission spectroscopy is also used to validate electron energy distribution measurements in the tail of the electron energy distribution function. Finally, changes in measured anode power flux as a function of transverse magnetic field are determined so that the magnitude of larger anode fall voltages can be put into perspective from a power balance standpoint.

III. EXPERIMENTAL SETUP

The discharge apparatus illustrated in Fig. 1 is mounted in a 1 m diam by 1.2 m long cylindrical vacuum chamber that is evacuated by a National Research Corporation rotary gas ballast mechanical pump with a pumping speed of 400 cubic feet per minute. As measured by the chamber thermocouple gauge, once the ultimate pressure of 30 mTorr is reached, the tank is then filled to roughly one Torr of argon

and flushed several times before the discharge is ignited. Typical operating pressures with the discharge on range between 40 and 50 mTorr.

A gas-fed hollow cathode of the type utilized in many electric propulsion systems is used as the electron source for the discharge. Argon is the working gas for all experiments. The water cooled stainless steel anode is a 2.5 cm diam disk that is thermally and electrically isolated from the electromagnet gantry that it is mounted to. The anode is placed within an alumina sleeve, such that its only exposed surface is the front plane facing the cathode. For these experiments, the interelectrode gap is set to 6.0 cm. The temperature of the anode is monitored via thermocouples attached to the rear of the electrode. The electromagnet, with its shaped pole pieces, immerses the anode and the near-anode region in uniform magnetic field with the flux lines running parallel to the anode surface. Before the experiment, the magnetic field is measured at the anode surface with a gaussmeter to obtain a calibration curve that is used to correlate the electromagnet coil current to the applied field. The region of uniform magnetic field extends to over three centimeters above the surface of the anode. In discharges of this type, current transport is dominated by transverse diffusion.

The discharge is initiated by first preheating the hollow cathode and then applying high voltage between the cathode and a tantalum auxiliary electrode. Once ignited, the arc is transferred to the stainless steel anode and is operated in a constant current mode. After the transfer, the initial attachment at the anode usually consists of a very localized spherical spot at the anode surface. It has been found that a weak transverse magnetic field of $\sim$10 G tends to smear out the spot so that the attachment at the anode is uniform. Though a subject of another investigation, the mechanism behind the formation of this initial anode spot may be due to anode surface nonuniformity, which tends to concentrate the electric field locally. The transverse magnetic field acts to smear out these effects because it limits transverse diffusion, thus forming a more uniform electron collection surface so that local anode spot attachments are no longer favored. In other words, because transverse electron flux decreases with an increasing magnetic field, a localized attachment at the anode can no longer be supported, and thus in order to sustain the discharge at constant current, electron collection must take place over a larger portion of the anode surface.

For this investigation, a 9.25 A arc is maintained between the cathode and anode. This operating point gives rise to an anode current density of roughly 2 A/cm^2, which simulates conditions at the anodes of steady-state 100 kW class MPD thrusters.[8]

This study utilizes invasive Langmuir probe techniques and noninvasive emission spectroscopy methods. The Langmuir probe collection surface used in this investigation consists of a 3 mm long tungsten wire that is 0.2 mm in diameter. The unexposed portion of the tungsten wire is isolated from the discharge via an alumina sheath. The probe is oriented such that its axis is parallel with the magnetic field lines. The probe is located 2.5 mm above the anode surface. The spatial extent of the anode fall region is assumed to be on the order of a Debye length, which for this study ranged

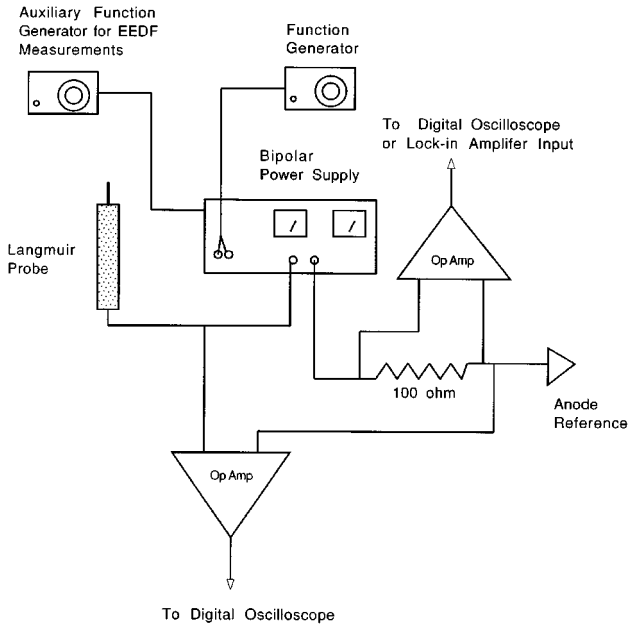

FIG. 2. Langmuir probe circuit.

from 1 to 10 μm. The probe was in all cases outside the anode sheath and thus was not expected to disturb the anode sheath. The probe is connected to a programmable bipolar power supply that is driven by a signal generator so that a triangle wave of a few hertz is applied to the probe. The measured probe voltage and current are then sent to an operational amplifier, which in turn sends the signals to a Tektronix digital oscilloscope. The digital oscilloscope is used to acquire the traces so they can be extracted and stored on a personal computer via a National Instruments General Purpose Interface Bus (GPIB) interface. In addition to standard Langmuir probe data, electron energy distribution data are also taken. To make these measurements, an additional signal generator is used to superimpose a 1 kHz, 1 V sine wave on the probe voltage. The probe current signal is then sent to a digital, dual-phase Stanford Research lock-in amplifier that is set to lock in on frequencies at the second harmonic of the 1 kHz superimposed signal. The lock-in amplifier output is then sent to the oscilloscope. The entire setup, including the computer, is plugged into isolation transformers. A block diagram of the Langmuir probe circuit is illustrated in Fig. 2. All Langmuir probe voltage measurements are made with respect to the anode. Representative plots corresponding to standard Langmuir probe measurements and electron energy distribution function (EEDF) measurements are illustrated in Figs. 3(a) and 3(b), respectively. Each plasma parameter determined from the $I-V$ characteristic of the Langmuir probe is actually the average of several Langmuir probe traces taken at the specified operating condition.

The emission spectroscopy setup Fig. 4 consisted of an iris, a concave/convex doublet, and a Spex 500M 0.5 m spectrometer fitted with a 1800 groove/mm holographic grating. The optics were arranged so the spectrometer collected light from a slice no more than 0.2 mm thick in front of the anode surface. The spectrometer scanned for argon neutral and

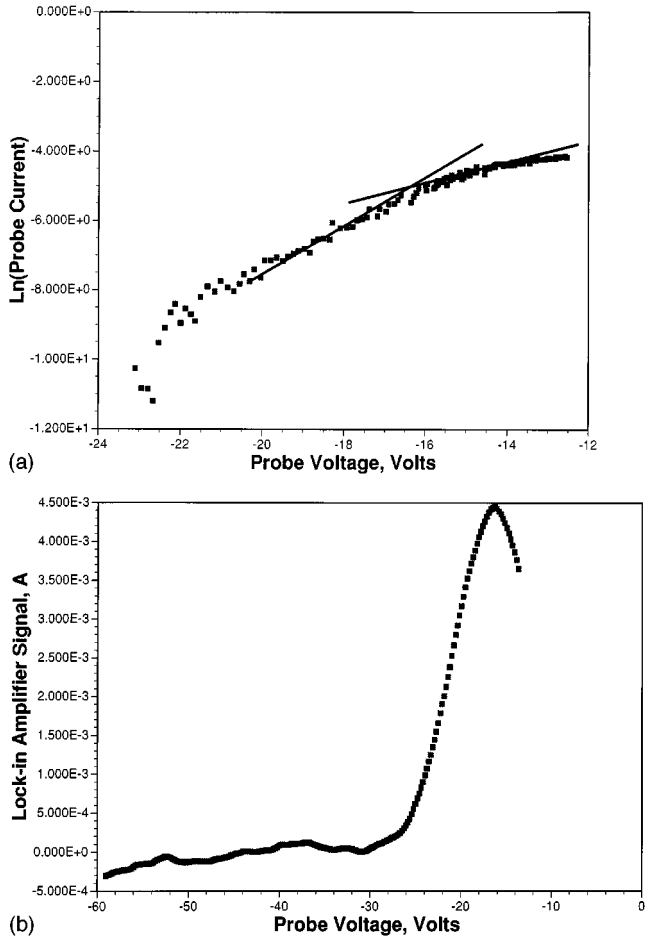

FIG. 3. (a) Typical Langmuir probe trace: 9.25 A argon discharge plasma, 52 mTorr, 18 G transverse magnetic field. (b) Typical lock-in amplifier signal for EEDF measurements: 9.25 A argon discharge plasma, 52 mTorr, 18 G transverse magnetic field.

ion lines located between 470 and 481 nm.

Water calorimetry is used to determine the rate at which energy is deposited into the anode. By measuring the temperature of the water entering the anode, the temperature of the water exiting the anode, and the water mass flow rate ($\dot{m}$), the rate at which heat is deposited into the anode can be calculated with

$$\frac{dQ}{dt} = c_v \cdot \dot{m} \cdot \Delta T, \tag{4}$$

where c_v is the specific heat of water at constant volume and ΔT is the water temperature change. The cooling water is provided by a Neslab recirculating chiller with a cooling capacity of 950 W. The water flow rate is measured by a standard spring loaded water flow meter. Though the main utility of the water calorimetry resides in the expedition of the heat flux measurements, it also afforded the opportunity to minimize electrode evaporation by removing excess thermal energy.

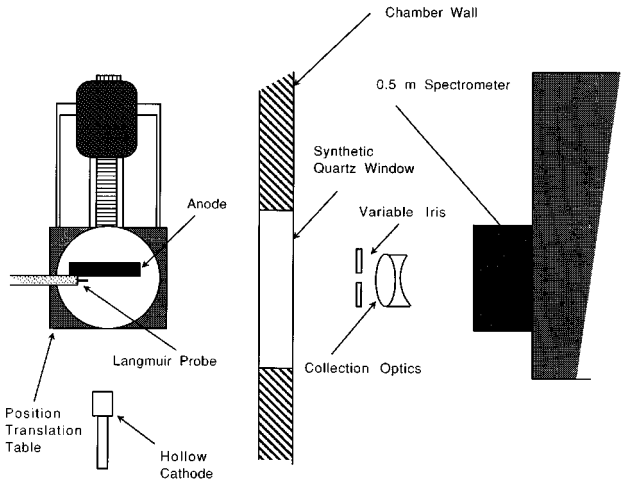

FIG. 4. Emission spectroscopy setup.

IV. LANGMUIR PROBE AND EMISSION SPECTROSCOPIC PROCEDURE

Langmuir probe data are acquired as mentioned above by recording collected plasma current as a function of imposed probe voltage. Because the ratio of the probe radius to estimated Debye length exceeds ten, thin sheath analysis applies. The electron number density is obtained from the ion saturation current, i_+, via the relation

$$i_+ = 0.61 \cdot e \cdot n_e \cdot \sqrt{\frac{Z_i \cdot kT_e}{M_i}}, \tag{5}$$

where n_e is the electron number density, Z_i is the charge state of the ion species, and M_i is the mass of the ion. Because the ion Larmor radius for operating conditions in this experiment is large compared with probe dimensions, magnetic field effects are not expected to significantly impact density measurements. The electron temperature is found by obtaining the slope from the most linear region of a semilog plot of current versus voltage for those voltage values above the floating potential. The electron temperature is then the reciprocal of this slope if the electron energy distribution is Maxwellian. The plasma potential is obtained by locating the ''knee'' of the semilog plot. In general, the intersection of the electron retarding region and the electron saturation region is taken to be the ''knee.'' [9] Though visible in the semilog plot, the knee in the raw current–voltage characteristic was not as evident, owing to a poorly saturating probe.

The electron energy distribution function is obtained by using the widely accepted technique of superimposing a small signal onto the probe voltage.[10] A subsequent Taylor expansion of the measured current yields terms that are proportional to the various derivatives of the probe current. The lock-in amplifier detects the second harmonic of the current signal, which is proportional to second derivative of the probe current. Recall that the electron energy distribution function is proportional to the second derivative of the probe current,[11]

$$f(E) \propto \sqrt{E} \cdot \frac{d^2 I_p}{dV_p^2}.$$

In the Taylor expansion of the probe current, the second derivative term is proportional to the term containing the second harmonic of the small input ac signal. It is then a simple matter to obtain this second harmonic via a lock-in amplifier. The estimated error in the EEDF measurements is approximately 8%.[12] Most of the uncertainty in the EEDF measurements is associated with higher-order derivatives that contribute to the signal detected by the lock-in amplifier.

Experimental electron energy distribution functions, $f(E)$, can be fitted to the following relation:

$$f(E)=C\cdot\sqrt{E}\cdot\exp(-BE^n), \tag{6}$$

where E is the electron energy, C is a normalization factor, and B and n are fitting parameters. A Maxwellian distribution corresponds to an n value of 1 while a Druyveststyn distribution corresponds to an n value of 2.[12] Using this model for the electron energy distribution function, one can ascertain the nature of the distribution. Indeed, from a semilog plot of the lock-in signal versus probe voltage one can determine the nature of n. For example, if the plot of the $\mathrm{Ln}|A(E)|$ versus energy, where $A(E)$ is the lock-in signal, is linear then the EEDF is Maxwellian. Once n is known, B and a constant proportional to C can be obtained from a semilog plot of $\mathrm{Ln}[A(E)]$ versus energy raised to the appropriate power.

Emission spectroscopy measurements were carried out to characterize the near-anode plasma (see Fig. 4). One important aspect of the spectroscopic measurements is that of monitoring the growth or decay of the energetic electron population:

$$\frac{I}{n_e}=\mathrm{const}\cdot\int_{E_T}^{\infty}\sqrt{\frac{2E}{M}}\,\sigma(E)\cdot f(E)dE. \tag{7}$$

Here the ratio of the intensity, I, of a particular argon line to the local electron number density measured in that region is proportional to the excitation rate for that transition, which in turn is proportional to the fraction of those electrons with energies above the excitation threshold for that transition, as determined by integrating over the electron energy distribution function, $f(E)$. Here $\sigma(E)$ is the excitation cross section as a function of energy, E, and M is the mass of the emitting argon atom or ion. The excitation threshold, E_T, for the excitation of the argon neutral 470.2 nm line is 14.5 eV, whereas the excitation threshold for the excitation of the 480.6 nm argon ion line is 35 eV.[13] The emission spectroscopy data, therefore, complements the EEDF measurements.

V. RESULTS AND DISCUSSION

A. Anode fall and electron density variations with magnetic field

In general, one major aspect of this study is essentially to characterize how the anode sheath potential, known as the anode fall, varies with transverse magnetic field. This measurement is expedited by determining the plasma potential near the anode surface. If the potential variation across the positive column is fairly flat, then this technique can be used to approximate the anode fall. In this study, error in the anode fall measurements using this procedure was calculated to be less than 10%. Positive anode fall voltages as referred to here are associated with an electron attracting anode. As is seen from an examination of Fig. 5, the anode fall voltage is not strictly a monotonically increasing function of magnetic field, as would be expected. What instead is observed is a local maxima in the anode fall voltage, where additional increases in transverse magnetic field result in an abrupt decrease in the anode fall. After the sudden drop, it is observed that the anode fall voltage increases with magnetic field, but a much slower rate than before. The region where the anode fall increases with increasing transverse magnetic field appears to be in part related to the decrease in available electron flux, which, in general, should drop off as $1/B$ for Bohm-like diffusion or $1/B^2$ for classical diffusion.[14] It appears that other mechanisms may be at work to increase available flux in the near-anode region for those transverse field strengths that correspond to values beyond the anode fall maximum. In general, the magnitude of the available electron flux depends on ionization phenomena taking place in the main discharge column. This ionization is expected to be a function of the electron EEDF, which in general varies with bulk discharge conditions such as pressure, magnetic field, and discharge voltage. The transverse diffusion flux determines the steady-state value of the electron number density throughout the column and up to the anode sheath edge. The measured electron density near the sheath edge reflects the behavior of the available transverse flux with the changes in magnetic field. This relationship follows from the scaling between the charge production rate, density, and flux: $n_e\propto\dot{n}_e\propto\Gamma_e$. Here $\dot{n}_e$ is the charged pair production rate. This behavior is illustrated in Fig. 6, where the available transverse current is shown to vary linearly with electron number density. Here the available transverse current is approximated by using experimentally determined plasma parameters in the relation derived by Sugawara:

$$I_{e\perp}=\frac{1}{4}\,en_0\overline{\nu}\cdot A_p\cdot\left(\frac{16}{3}\cdot\frac{\lambda_e\cdot\alpha^{1/2}}{K(k)\cdot r_0}\right)\cdot\frac{1}{\{1+\frac{16}{3}\cdot(\lambda_e\cdot\alpha^{1/2})/[K(k)\cdot r_0]\}}, \tag{8}$$

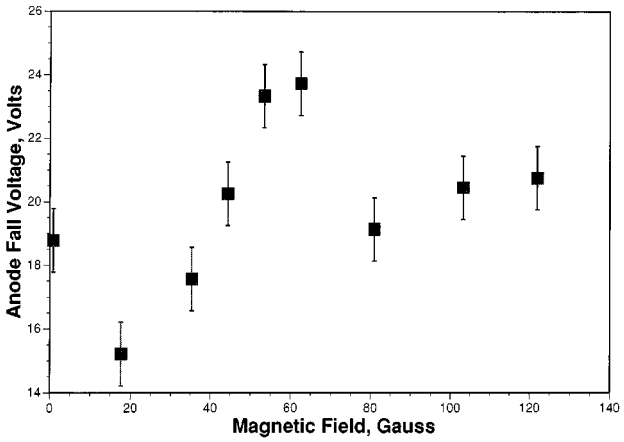

FIG. 5. Anode fall voltage variations with transverse magnetic field: 9.25 A argon discharge plasma, 52 mTorr.

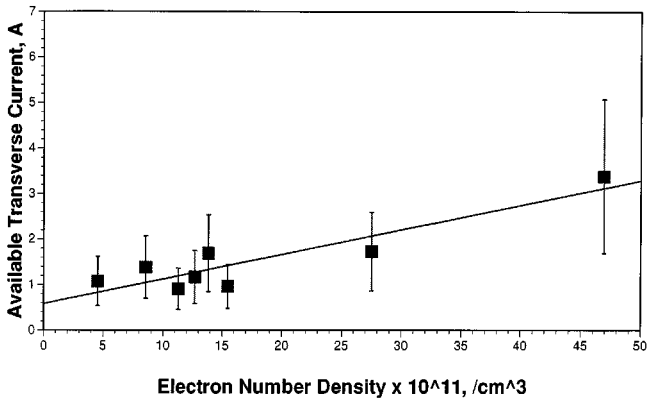

FIG. 6. Calculated available transverse current versus electron number density: 9.25 A argon discharge plasma, 52 mTorr.

where this relation describes the saturation current available to a planar probe for a given magnetic field strength.[15] Here, λ_e is the electron mean-free path, r_0 is the anode radius, A_p is the anode surface area, n_0 is the electron number density, and $K(k)$ is the elliptic integral of the first kind. The variable α is the ratio of the transverse diffusion coefficient to the diffusion coefficient when the magnetic field is zero and is proportional to the reciprocal of the Hall parameter in the limit of large magnetic field strength. It should be pointed out that the available current calculated by this relation is actually smaller than the discharge current. This underestimation is most likely attributed to the deviation in the true transverse diffusion coefficient from the classical behavior [see Eq. (2)] used in the Sugawara relation. This linear scaling of available current with electron density is fortunate in that the determination of density is not dependent on the large number parameters that are required to calculate available current in the presence of a magnetic field. It is interesting to note that the variations in the anode fall appear to be a response to changes in the transverse flux, as reflected in the related changes in the electron number density (compare Figs. 5 and 7). Indeed, for the portion of the plot where the anode fall is growing rapidly with increasing magnetic field, the electron number density is either slowly rising or slowly falling. The local minima in the electron number density corresponds to the local maxima in the anode fall voltage. Further increases in the transverse magnetic field results in a rather dramatic growth in electron number density, a trend that continues for increasing magnetic field. Under these conditions, the anode fall and discharge voltage are observed to saturate. These findings suggest that the changes in the local electron number density may be an indicator of expected anode fall voltage behavior as the transverse magnetic field is varied.

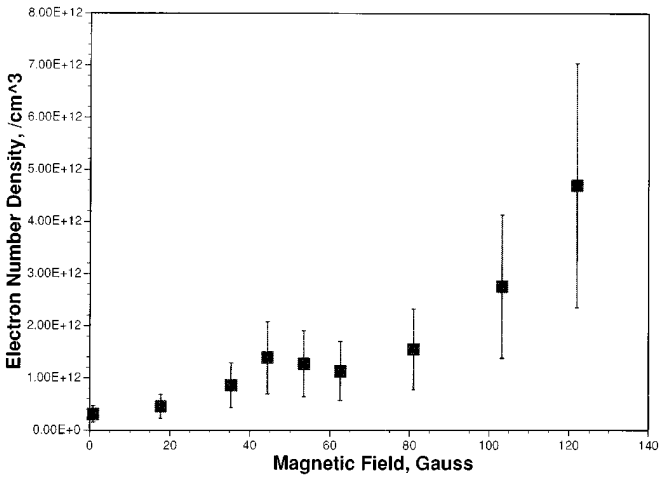

FIG. 7. Electron number density variations with transverse magnetic field: 9.25 A argon discharge plasma, 52 mTorr.

The actual mechanism of how anode fall growth occurs is subject to debate. One possible mechanism for anode fall evolution with a transverse magnetic field may be obtained by again examining the transverse flux. For the operating conditions where the transverse field is very small, the available transverse flux is large compared to the discharge current. Under these conditions, all of the electron flux that enters the anode sheath is not needed, and therefore is not collected. As a result, electron space charge accumulates at and near the anode surface. This electron space charge assumes a steady-state value as a consequence of the balance between entering charge and electron loss processes. The net result of the negative space charge is primarily to reduce that potential of the anode relative to the sheath edge thus decreasing the anode fall to a lower value as the ratio of available current to discharge current increases. The magnitude of the steady-state anode surface charge or near-anode space-charge depends on the available flux, which is in turn controlled by the transverse magnetic field. As the transverse magnetic field increases, the anode surface charge must decrease to a lower steady-state value if electron surface loss processes are constant. Decreases in this surface charge give rise to increases in the anode potential relative to the sheath edge, which essentially corresponds to an increase in the anode fall voltage. Thus, when the measured electron number density is slowly varying or decreasing in magnitude, the problems associated with the reduction in transverse flux is enhanced because the transverse diffusion coefficient is dropping, as is the case with an increasing transverse magnetic field and because local density growth is insufficient to offset the decrease in negative space charge in the anode sheath. Under these conditions, the anode fall voltage can be expected to increase with increasing transverse magnetic field. These trends are experimentally observed as is illustrated in Figs. 5 and 7. The measured jump in electron number density is associated with a jump in measured transverse flux and an increase in transverse flux gives rise to an increase in the uncollected negative space-charge density at the anode. This negative space charge reduces the potential of the anode relative to the sheath edge so that the measured drop and subsequent saturation of the anode fall with increasing magnetic field under these conditions is in accordance with the proposed model mentioned earlier.

It is interesting to note that the work of Diamant *et al.*[16] discusses experimental findings that allude to the importance of electron number density near the anode in a pulsed MPD thruster. The Diamant *et al.* study asserts that at large anode

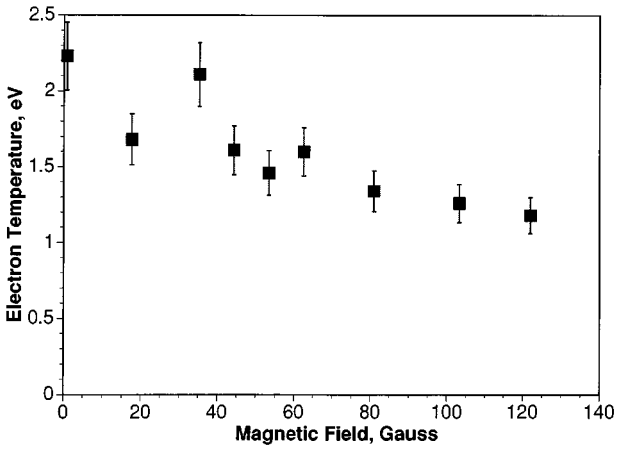

FIG. 8. Langmuir probe electron temperature variations with transverse magnetic field: 9.25 A argon discharge plasma, 52 mTorr.

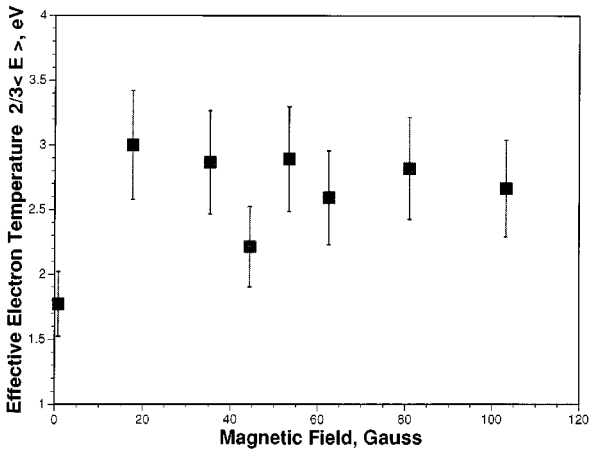

FIG. 9. Effective electron temperature variations with transverse magnetic field: 9.25 A argon discharge plasma, 52 mTorr.

falls, a transition into a spot mode attachment ensues, which essentially functions to evaporate anode surface material. Ionization of this metal vapor is postulated to increase the number of charge carriers in the near anode-region and to ultimately prevent subsequent increases in the anode fall, thus leading to a saturation in anode sheath potential. In this respect, anode surface vaporization and subsequent ionization of the metal vapor controls the anode fall in the spot mode. This finding is consistent with observations in this study, where variations in the anode fall voltage appear to occur with changes in the local electron number density. In this case, however, the effect of the magnetic field on ionization rate (see Sec. V B) controls charge carrier production in the near-anode region as opposed to the vaporization processes discussed in the Diamant *et al.* study.

B. Electron energetics and ionization phenomena

The measured electron temperature appears to decrease with increasing magnetic field. Although this measured decrease is fairly slight (see Fig. 8), this behavior appears to suggest that the plasma is cooling as it diffuses across field lines on its journey to the anode. In order to reach the anode, the electrons must undergo a collisional ''random walk'' to the anode. Through each collision with a neutral or ion, there is an opportunity for the electron to liberate a fraction of its energy. Because the transverse drift distance between collisions of an electron in a magnetic field is on the order of a Larmor radius, the distance that an electron will travel between collisions decreases with increasing magnetic field; as a result, the rate at which electrons lose energy via collisions with slow ions and neutrals can be expected to increase as the transverse magnetic field increases. It is important to note that the trends in average electron energy as measured using the EEDF, as illustrated in Fig. 9, does not appear to corroborate with the Langmuir probe measurements. An effective electron temperature is obtained from the average energy resulting in an integration over all energies using the measured EEDF. EEDF measurements suggest that the electron temperature profile as a function of magnetic field is actually flat. This flatness suggests that for most conditions the energy obtained from the discharge electric field balances the energy lost due to inelastic collisions with neutrals and ions. Also, EEDF measurements suggest that the magnitude of the average energy is actually a factor of 2 larger than that measured using standard Langmuir probe theory. These differences between the electron temperature behavior and magnitude may be related to the fact that the measured EEDFs are not Maxwellian (see Fig. 10) as is assumed in single Langmuir probe theory, but instead Druyvesteyn-like (see Fig. 11); here the energy exponential is 2 instead of 1. Distributions of this nature are associated with significant fractions of the electron populations having their energies close to the average energy. Also, it should be pointed out that care must be taken in interpreting the fits here because deviations from experimental data at higher energies are significant.

Also observed was the expansion of the electron energy distribution function to higher energies as the magnetic field increases. This observation, displayed in Fig. 12, suggests that an increasing amount of the discharge power is coupled into the plasma as the magnetic field becomes larger. This assertion appears to be supported by the anode heat flux measurements, which indicate that the fraction of discharge power associated with anode losses decreases with increasing magnetic field strength, suggesting that as the magnetic field increases, an increasing fraction of the input power goes directly into the plasma as opposed to the anode.

It should be pointed out that deviations from this Druyvesteyn-like form are seen in the tails of these electron energy distribution functions (see Fig. 12). Peak structure observed to be present in the tails of the EEDFs may be remnants of an electron beam component associated with the cathode fall. This beam component may be necessary to sustain the ionization processes needed to maintain the discharge. The observed suppression of these components with increases in applied magnetic field strength appears to be a consequence of the magnetic field enhancing the coupling of the beam component to the gas. The observed increases in plasma density and the associated saturation of the anode fall voltage under such conditions may be a consequence of this coupling. The basis of this coupling appears to be related to

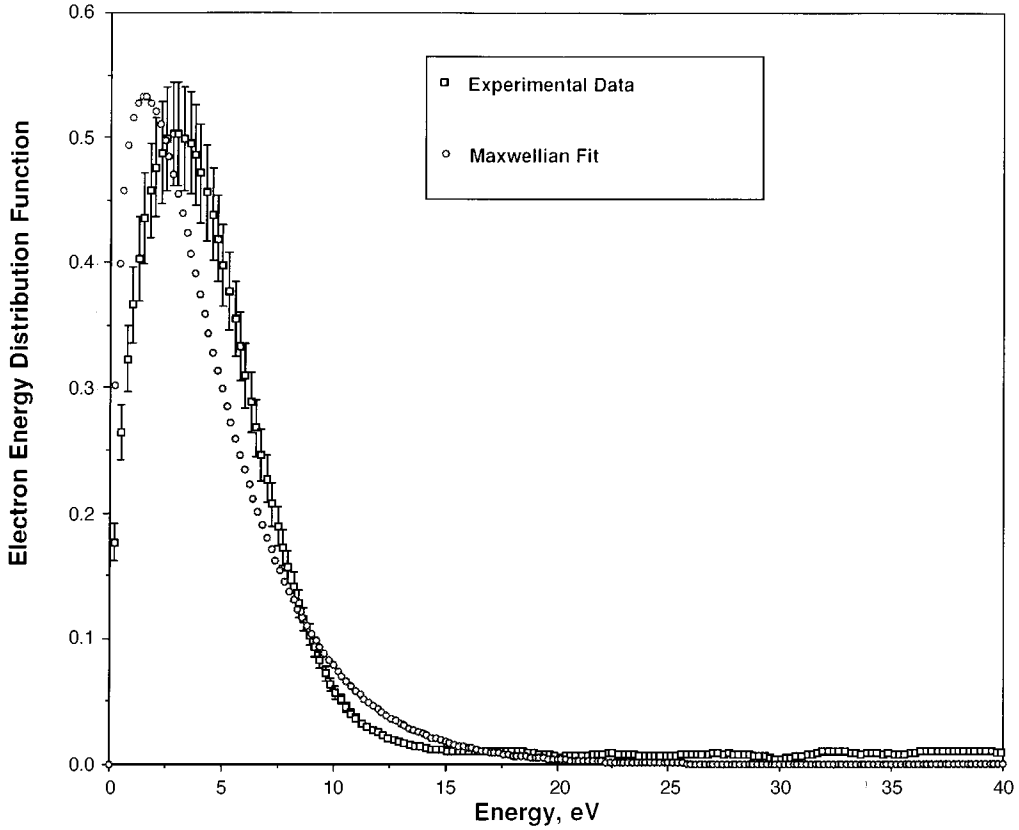

FIG. 10. Indication of a non-Maxwellian electron energy distribution function: 9.25 A argon discharge plasma: 35 G transverse magnetic field, 52 mTorr.

increases in the electron residence time in the discharge with increasing transverse magnetic field strength. This increased residence time enhances the probability for an electron to have a thermalizing collision with an electron from the cooler, bulk population or an inelastic collision with a neutral particle, thus smoothing out the bumps in the tail by transporting energy out of these higher-energy regions. These observations allude somewhat to the notion that an electron beam component may be useful in reducing the growth of the anode fall due to its ability to enhance ionization rates.

The EEDF measurements are used in the calculation of ionization rates in the near-anode region as a function of transverse magnetic field. The ionization rate per electron was calculated at a given transverse magnetic field by using the low-energy electron ionization cross section data from

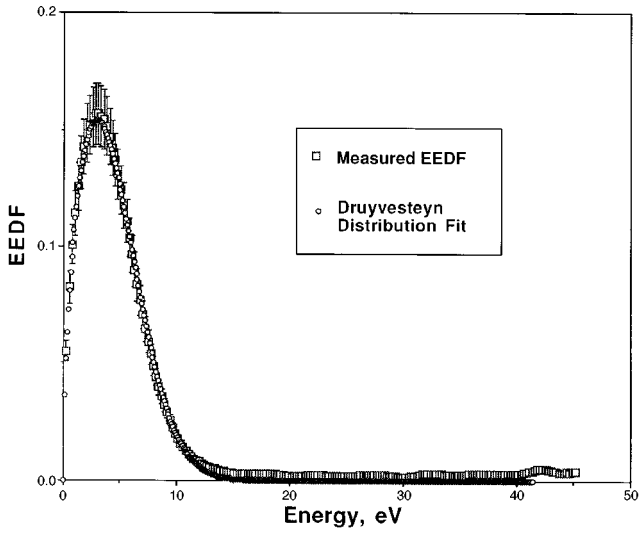

FIG. 11. Druyvesteyn-like EEDF: 9.25 A argon discharge plasma, transverse magnetic field: 35 G, 52 mTorr.

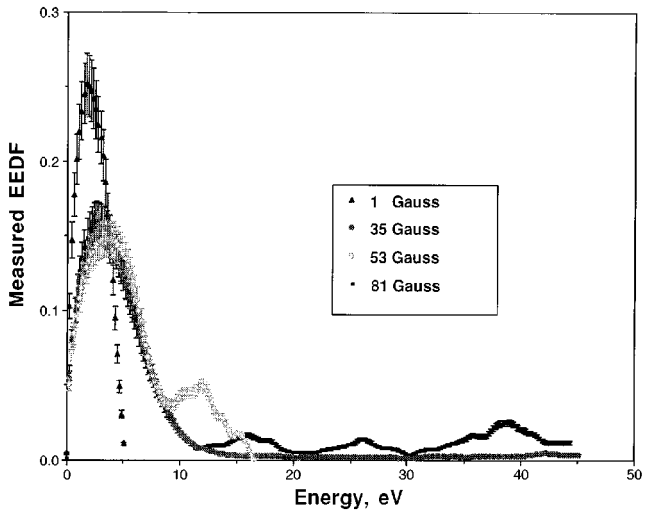

FIG. 12. Near-anode EEDF variations with transverse magnetic field: 9.25 A argon discharge plasma, 52 mTorr.

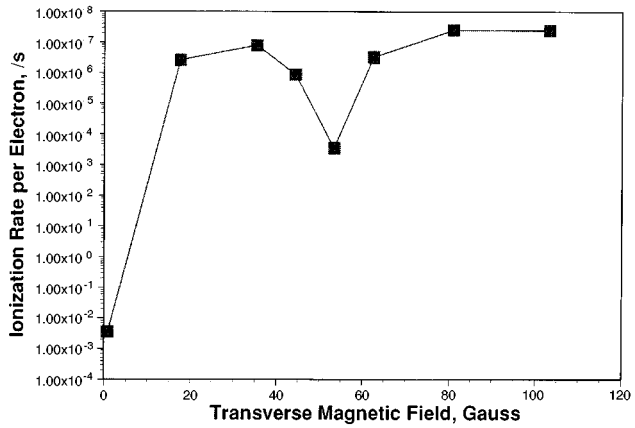

FIG. 13. Variations in near-anode ionization rate with transverse magnetic field: 9.25 A argon discharge plasma, 52 mTorr.

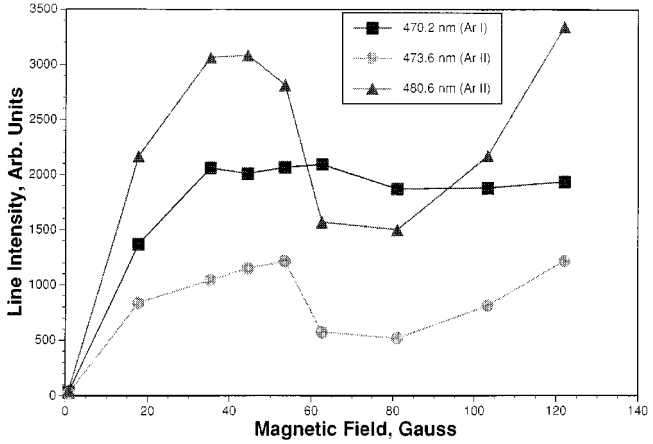

FIG. 14. Near-anode variations in argon spectral line intensity with transverse magnetic field, 9.25 A argon discharge plasma, 52 mTorr.

Rapp and Golden-Englander[17] in the following relation:

$$K = n_{\text{gas}} \cdot \int_{E_T}^{\infty} \sigma(E) \cdot \sqrt{\frac{2E}{M}} \cdot f(E) \cdot dE. \tag{9}$$

Because the magnitude of the ionization frequency controls charge production, changes in this rate should be reflected in changes in the measured anode fall voltage. That is, it is to be expected that when the ionization frequency as a function of transverse magnetic field is decreasing, the rate at which the anode fall grows with magnetic field should increase. Figure 13 illustrates the response of the experimentally estimated ionization rate per electron to changes in transverse magnetic field strength in the near-anode region. It should be pointed out that the changes in anode fall voltage as a function of transverse magnetic field roughly follow the observed trends in the near-anode ionization rates. It is also worth noting that a local minimum in the ionization rate approximately corresponds to the local maximum in the anode fall voltage. Also, the ionization rate appears to flatten out at the higher magnetic field strengths, even though the measured electron number density increases quite dramatically. This relative flatness of the ionization rate at the higher field strengths is due to the nonvarying shape of the electron energy distribution functions in this range, which translates into average energies and ionization path-lengths that are also similar. What is not so similar between the operating points at higher magnetic field strengths, however, is the Hall parameter (ω_{ce}/υ). The Hall parameter is a measure of how many orbits an electron executes about its guiding center between collisions. The total distance the electron must travel, including the distance traveled along the gyro-orbits between collisions, is significantly different due to increases in the Hall parameter as the magnetic field increases. Indeed, increases in the effective path length due to the application of a transverse magnetic field has been exploited to enhance the ionization probability in hollow cathode discharges.[18] Therefore, if the ionization mean-free paths are similar for the electrons at the 81 G data point and the 103 G data point, then the operating conditions in which the electron is forced to transverse a longer total distance to the anode due to gyrorotation will generate, in general, more electrons than in the case of an electron traveling a shorter total distance to the anode. The measured increase in electron number density at the 103 G data point relative to the 81 G data point is then expected.

Variations in the intensity of two argon ion lines and one argon neutral line in the 0.2 mm imaged volume of plasma adjacent to the anode appear to be related to changes in the local electron number density. The spectral behavior is illustrated in Fig. 14. The puzzling aspect of these data, however, is related to the observation that for a range of magnetic field strengths the behavior of the neutral line appears to be fairly flat while the ion line intensities vary significantly under the same conditions. The intensity of the argon ion lines correlate best with the measured changes in near-anode electron number density. One explanation for the sensitivity of the argon ion lines to changes in discharge conditions as opposed to the apparent insensitivity of the neutral lines measured under the same conditions resides in the very nature of the neutral emission. In general, ion emission lines reflect the ion production rate because these newly formed ions can also be also excited in the ionization process. In this respect, the ion lines provide density information convoluted with additional information on electron energetics. Argon neutral lines, on the other hand, are not expected to provide much information on electron densities or production rates because such lines reflect only the population of electrons with energies above the excitation threshold of that particular line.

Also measured was the rate of growth of energetic electrons as a function of transverse magnetic field (see Fig. 15). This measurement is accomplished by normalizing the measured spectral intensity to the electron number density. This quantity [see Eq. (7)] is proportional to the fraction of those electrons with energies above the excitation threshold for a specified transition. As mentioned earlier, the excitation threshold for the neutral line 470.2 nm is 14.5 eV while the excitation threshold for the ion line 480.6 nm is 35 eV. In general, with the exception of the initial jump for small transverse magnetic fields, the fraction of energetic electrons decreases with increasing magnetic field. However, as the

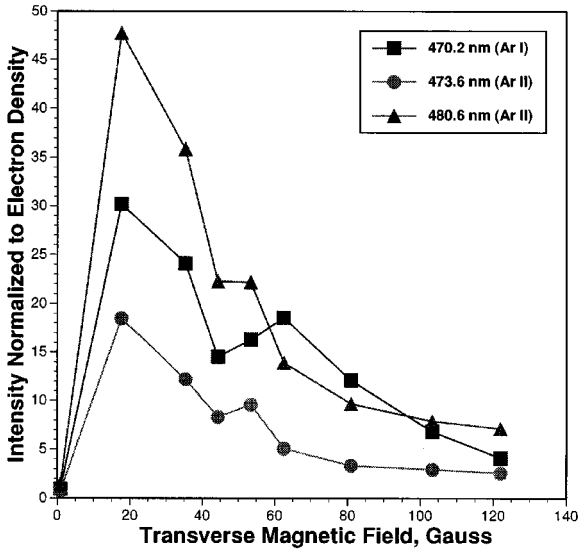

FIG. 15. Variations in spectral intensity of select argon lines normalized to local electron number density as a function of transverse magnetic field.

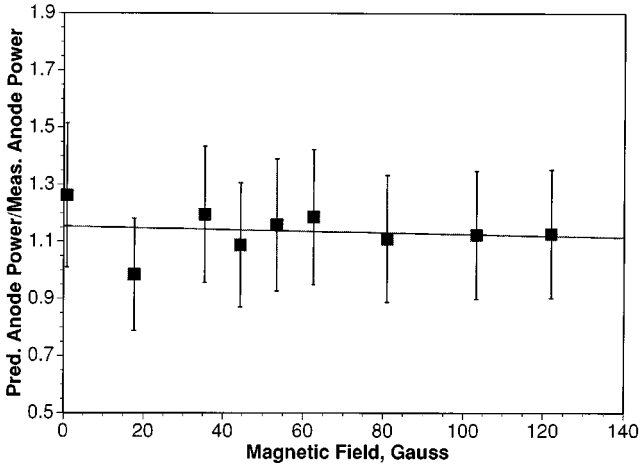

FIG. 16. Degree of agreement between the anode power model and the measured anode power deposition: 9.25 A argon discharge plasma, 52 mTorr.

magnetic field associated with the local maximum in the anode fall is approached from lower field strengths, there does appear to be growth in the electron population with energies above 14.5 eV. This assertion is based on the observation of local growth in the electron density normalized intensity of the argon 470.2 nm neutral line with increasing transverse magnetic field. EEDF measurements indicate additional structure in the higher-energy region when the anode fall is at its maximum, which is consistent with the observed spectra, especially for those electrons with energies over 12 eV. Beyond this critical magnetic field strength of 63 G (associated with the large anode fall), the rate at which the population of the high-energy electrons decreases with increasing magnetic field is reduced somewhat.

C. Measured anode power deposition

Measured anode power deposition determined via water calorimetry correlates well with variations in the energy balance model:[19,20]

$$P_A = I_d \cdot \left(\frac{5kT_e}{2e} + V_A + \phi_{\mathrm{wf}} \right) + P_c + P_r . \tag{10}$$

Here the total power deposited into the anode, P_A, can be divided into an electronic term, which consists of the discharge current, I_d, multiplied by an electron thermal energy term that is proportional to T_e, an anode sheath potential term, V_A, and a work function term, Φ_{wf}. Also included in the equation is P_c, which accounts for convection, and P_r, which accounts for radiation from the plasma and the glowing cathode. This model has been shown to represent the power flux into the anode of MPD thrusters quite well.[8,20] The deviation between the measured anode power flux and the expected heat flux, as calculated using the energy balance relation was found to be on the average roughly 20% (see Fig. 16). The overestimation of the predicted anode flux may be due to the uncertainty in the work function. The work function of iron was used in the equation for the stainless steel. Given the variations in the work functions of the components that make up the stainless steel alloy, the error contribution associated with using the work function of the stainless steel should not exceed 3%.[21] Another source of error could be due to thermocouple inaccuracies in which temperature measurements could be off by as much as 0.6 °C. This error in temperature contributes a power flux measurement error of roughly 20%.

The anode fall contribution, $I_d \cdot V_A$, in which V_A is the anode fall voltage, as measured by the Langmuir probe, was always on the order of 80% of the measured anode power flux, thus dominating anode power deposition. The fact that this term appears to dominate is best illustrated in Fig. 17. Here the trends in measured anode heat flux are seen to correlate quite well with variations in the product $I_d \cdot V_A$.

The fraction of total discharge power that is associated with the anode heat flux decreases linearly with increasing magnetic field strength (see Fig. 18). Again, this suggests that a larger fraction of the input power is being coupled into

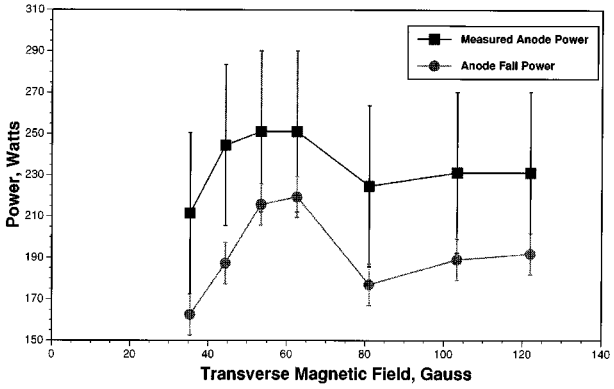

FIG. 17. Trends between measured anode power deposition and anode fall power: 9.25 A argon discharge plasma, 52 mTorr.

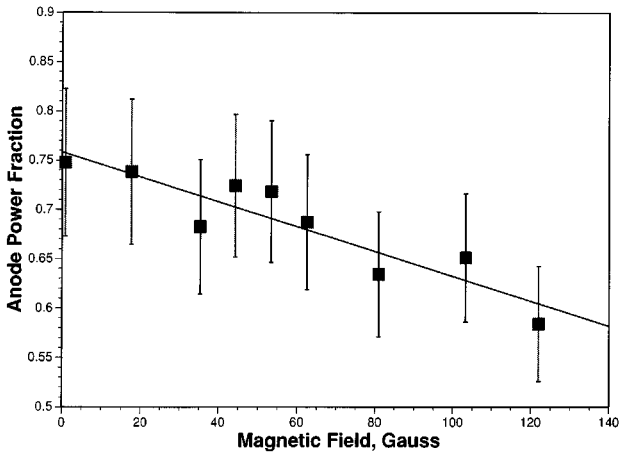

FIG. 18. Measured anode power fraction variations with transverse magnetic field: 9.25 A argon discharge plasma, 52 mTorr.

the plasma rather than the anode as the magnetic field is increased. It should be pointed out that similar behavior is observed in MPD thrusters.[1]

VI. CONCLUSIONS

The main purpose of this work is to emphasize the proposed relationship between electron number density and anode fall voltage based on experimental observations and phenomenological arguments. The measured variations in the anode fall voltage appear to be related to changes in the electron number density. This assertion, based on supporting data, is readily explained. The electron density at the sheath edge is proportional to the transverse flux. It is this flux that ultimately determines the space-charge distribution and the potential distribution in the anode sheath. This potential distribution defines the anode fall voltage. The measured variations in electron number density with transverse magnetic field can be attributed to changes in the ionization rate as the magnetic field is varied. It then follows that external modification to ionization processes in the near-anode region may be one means of controlling and ultimately reducing the anode fall voltage.

[1]R. Myers, *Proceedings of the 1991 AIAA Joint Propulsion Conference*, AIAA-91-2342 (American Institute of Aeronautics and Astronautics, Washington, DC, 1991).
[2]A. Gallimore, A. Kelly, and R. Jahn, AIAA J. Propulsion Power **9**, 361 (1993).
[3]W. Schall, *Proceedings of the AIAA 9th Electric Propulsion Conference*, AIAA-72-502 (American Institute of Aeronautics and Astronautics, Washington, DC, 1972).
[4]H. Tahara, M. Sasaki, Y. Kagaya, and T. Yoshikuwa, *Proceedings of the AIAA 21st International Electric Propulsion Conference*, AIAA 90-2554 (American Institute of Aeronautics and Astronautics, Washington, DC, 1990).
[5]J. T. Scheuer, R. P. Hoyt, K. F. Schoenberg, R. A. Gerwin, R. W. Moses, I. Henins, R. M. Mayo, and D. C. Black, *AIAA 23rd International Electric Propulsion Conference*, IEPC-93-118 (The Electric Rocket Society, Columbus, OH, 1993).
[6]G. Soulas and R. Myers, *23rd International Electric Propulsion Conference*, IEPC-93-194 (The Electric Rocket Society, Columbus, OH, 1993).
[7]H. Hugel, IEEE Trans. Plasma Sci. **PS-8**, 437 (1980).
[8]A. Gallimore, R. Myers, A. Kelly, and R. Jahn, AIAA J. Propulsion Power **10**, 262 (1994).
[9]J. Swift and M. Schwar, *Electrical Probes for Plasma Diagnostics* (Lliffe Books, New York, 1970), Chap. 1, Sec. 1.5, and Chap. 12, Sec. 12.6.
[10]H. Rundle, D. Clark, and J. Dechers, Can. J. Phys. **51**, 144 (1973).
[11]M. Druyvesteyn, Z. Phys. **24**, 781 (1930).
[12]J. E. Heidenreich, III and J. R. Paraszczak, J. Vac. Sci. Technol. B **6**, 286 Jan/Feb (1980).
[13]T. Cox, V. I. Deshmukh, D. O. Hope, A. J. Hydes, N. J. Braithwaite, and M. P. Benjamin, J. Phys. D **20**, 820 (1987).
[14]F. Chen, *Introduction to Plasma Physics and Controlled Fusion* (Plenum, New York, 1984), Chap. 5, Sec. 5.10.
[15]M. Sugawara, Phys. Fluids **9**, 797 (1966).
[16]K. D. Diamant, E. Y. Choueiri, and R. G. Jahn, *25th International Electric Propulsion Conference*, IEPC-95-234 (The Electric Rocket Society, Columbus, OH, 1995).
[17]D. Rapp and P. Englander-Golden, J. Chem. Phys. **43**, 1464 (1965).
[18]H. Kerkow, D. Boubetra, and K. Holldack, Nucl. Instrum. Methods Phys. Res. B **68**, 41 (1992).
[19]J. Cobine and E. Burger, J. Appl. Phys. **26**, 895 (1955).
[20]K. Shih and E. Pfender, AIAA J. **8**, 211 (1970).
[21]D. R. Lide, Editor in Chief, *CRC Handbook of Chemistry and Physics* (CRC, Ann Arbor, 1994), pp. 12–113.